THE ASTROPHYSICAL JOURNAL, 463:365–371, 1996 May 20

ON THE DYNAMICS OF SMALL-SCALE SOLAR MAGNETIC ELEMENTS

T. E. BERGER
Center for Space Science and Astrophysics, ERL 328, Stanford University, Stanford, CA 94305
AND
A. M. TITLE
Lockheed Palo Alto Research Laboratory, Department 9130, 3251 Hanover Street, Palo Alto, CA 94304
Received 1995 September 8; accepted 1995 November 30

ABSTRACT

We report on the dynamics of the small-scale solar magnetic field, based on analysis of very high resolution images of the solar photosphere obtained at the Swedish Vacuum Solar Telescope. The data sets are movies from 1 to 4 hr in length, taken in several wavelength bands with a typical time between frames of 20 s. The primary method of tracking small-scale magnetic elements is with very high contrast images of photospheric bright points, taken through a 12 Å bandpass filter centered at 4305 Å in the Fraunhofer "G band." Previous studies have established that such bright points are unambiguously associated with sites of small-scale magnetic flux in the photosphere, although the details of the mechanism responsible for the brightening of the flux elements remain uncertain. The G band bright points move in the intergranular lanes at speeds from 0.5 to 5 km s^{-1}. The motions appear to be constrained to the intergranular lanes and are primarily driven by the evolution of the local granular convection flow field. Continual fragmentation and merging of flux is the fundamental evolutionary mode of small-scale magnetic structures in the solar photosphere. Rotation and folding of chains or groups of bright points are also observed. The timescale for magnetic flux evolution in active region plage is on the order of the correlation time of granulation (typically 6–8 minutes), but significant morphological changes can occur on timescales as short as 100 s. Smaller fragments are occasionally seen to fade beyond observable contrast. The concept of a stable, isolated subarcsecond magnetic "flux tube" in the solar photosphere is inconsistent with the observations presented here.

Subject headings: MHD — Sun: faculae, plage — Sun: magnetic fields — Sun: photosphere

1. INTRODUCTION

Early high-resolution observations of small-scale solar magnetic field concentrations outside of sunspots were made by Sheeley (1967) using spectroheliograms taken at the Mount Wilson Observatory. The observations implied that the small-scale field elements possessed strong magnetic fields, as indicated by the presence of "gaps" in the spectral lines of Zeeman-sensitive transitions. Beckers & Schröter (1968), using spectrographic observations obtained at the Sacramento Peak Observatory, quantified the line splittings using Unno-Rachovsky line profile synthesis to show that the gaps imply magnetic field strengths of between 1100 and 1300 G. Chapman & Sheeley (1968) and Sheeley (1969) further established that the nonsunspot magnetic field in the photosphere forms a bright network when observed in weak line cores and the CN bandhead at 3883 Å, and that this network coincides with, but has a finer spatial scale than, the chromospheric network seen in the Ca II K line.

Spectroheliogram observations require scanning periods on the order of 10 s to build up two-dimensional images; atmospheric seeing changes, which typically occur on 10–100 ms timescales, thus cause excessive focus and distortion variations across the resulting images. In order to obtain uniform image quality for the study of small-scale magnetic structures, Dunn & Zirker (1973) developed single-exposure filtergrams in the wings of the Hα line. The resulting images revealed that the photospheric network seen in any single image is composed of discrete subarcsecond bright points and "filigree" or elongated chains of bright points. Mehltretter (1974) observed similar bright points in the far wings of the Ca II K line and found that their mean size is on the order of 0.″3 (about 200 km FWHM). Simon & Zirker (1974) found that at 0.″5 resolution photospheric bright points have a definite spatial correlation with, but are somewhat smaller than, the magnetic field structure inferred from simultaneous magnetograms. The vacuum refractor telescope at the Pic-du-Midi Observatory for many years produced the highest resolution observations of bright points in the photospheric network (Muller 1975; Muller & Keil 1983; Muller & Roudier 1984; Muller 1994). Observations from the Pic-du-Midi instrument confirm the existence of highly compact, isolated bright points with angular sizes ranging from 0.″22 to 0.″6. Berger et al. (1995) studied plage magnetic fields using the Swedish Vacuum Solar Telescope (SVST) and showed that although the size range of bright points in plage is slightly larger than that found in the network, the majority of elements consist of circular structures with 200 km diameter. The observations also confirmed that filigree seen at the resolution limit of the SVST are composed of strings of smaller bright points, as was recorded earlier in the speckle interferometric observations of de Boer & Kneer (1992).

Parallel to the imaging efforts, novel spectroscopic techniques were developed in order to refine magnetic field strength measurements outside of sunspots. The magnetic line-ratio (MLR) technique (Howard & Stenflo 1972; Frazier & Stenflo 1972; Stenflo 1973), as well as measurements of fully Zeeman split infrared lines (Harvey & Hall 1975; Zayer, Solanki, & Stanflo 1989), confirmed the existence of kilogauss magnetic fields in the photospheric

network and showed that more than 90% of the solar magnetic flux outside of sunspots or pores is in this "strong field" form. Stenflo (1973) measured aperture-dependent field strengths between 1100 and 2300 G. Tarbell & Title (1977) used Fourier transform techniques (Title & Tarbell 1975) to infer that average magnetic field strengths of 1200 ± 200 G exist at all sites where the spatially averaged field exceeds about 125 G. Stenflo & Harvey (1985) showed that the inferred field strength has only a weak dependence on the filling factor of the magnetic elements outside of spots. More recently, Keller et al. (1990) have used high-resolution filtergrams to compute MLR field strengths of 1000 G at the formation level of the Fe I 5250 Å line. These results are claimed to be consistent with a unique value for the field strength of magnetic elements in the photosphere; i.e., there is no need to introduce a distribution of field strengths to explain the observations. Rabin (1992) used an imaging near-infrared magnetograph for direct measurement of field strength in the Zeeman-dominated Fe I 15650 Å line. In contrast to Keller et al. (1990), Rabin measures field strengths ranging from 1000 to 1700 G in a plage region. Solanki (1993) reviews the various attempts to constrain the field strength of small-scale magnetic elements and concludes that the current set of measurements imply a strength between 1500 and 1700 G at the $\tau_{5000} = 1$ level of the standard quiet atmosphere.

Combined with the high-resolution imaging observations, the relative unanimity of the spectral measurements suggests that the strong component of the magnetic field outside of sunspots and pores is concentrated in isolated "flux tubes" of about 200 km in diameter with kilogauss field strength.[1] In fact, the flux tube concept has become the dominant theoretical paradigm of solar magnetic structure on all spatial scales. Spruit & Zweibel (1979) refined the "thin flux tube" model of Spruit (1976) to produce what has become the standard theoretical model of small-scale magnetic flux in the solar photosphere. The model is characterized by the balance of magnetic and *static* gas pressures across a well-defined boundary region of the flux tube. This static balance results in significant radial expansion of the flux tube with increasing height in the *hydrostatic* atmosphere.

The present flux-tube concept has largely developed through the observation of single images in time and through hydrostatic solutions to the MHD equations. As a result, the flux-tube solution is inherently a stationary one, which hypothesizes a single coherent magnetic entity which does not change substantially throughout its lifetime. Obviously this is a simplistic model which has only recently begun to be expanded through the numerical solution of the full set of two-dimensional, compressible, magnetohydrodynamic equations. For example, Steiner et al. (1994) model the effects of the granular convective flow field on a single thin flux "sheet" (a strictly two-dimensional element) in the photosphere. Their simulations predict that the effect of the granular convection is to induce "bending" mode oscillations of the flux tube, with a characteristic timescale of about 5 minutes. As a consequence of the oscillations, the intensity observed in the flux tube from any particular line of sight is predicted to oscillate on the same 5 minute timescale. Ryutova, Kaisig, & Tajima (1995) have performed plasma-dynamic simulations of the interaction of a single flux tube with an acoustic wave train. Their simulations predict that the flux tube should undergo a complex fragmentation process resulting in several smaller flux tubes being produced on a timescale commensurate with the period of the wave train.

Observational tests of such numerical predictions have only recently become possible using high-speed image acquisition methods during periods of exceptionally good seeing. Currently, the most successful technique for dynamic observations at small spatial scales uses real-time seeing evaluation and image selection with large-format CCD cameras at the SVST (Scharmer 1989). Title et al. (1989) have demonstrated the ability to image large fields of view (on the order of $100'' \times 100''$) with subarcsecond spatial resolution using this system. Simon et al. (1994) have produced an 11 hr long time series of continuum observations of quiet granulation in which a large majority of frames achieve 0".3 spatial resolution. Use of the solar optical universal polarimeter (SOUP) (Title & Rosenberg 1981) filter in combination with the real-time image selection system has produced high-resolution "movies" of the solar photosphere in several wavelength regimes with temporal separations on the order of seconds (Title et al. 1989; Title et al. 1992). These studies have produced the first high-resolution time series of near-simultaneous magnetogram, continuum, Hα, and Ca II K line images. Yi & Engvold (1993) used this system to show that photospheric bright points exist without exception at sites of magnetic flux through the photosphere, and are also preferentially located in convergent points in the mesogranular flow field. These results, in confirmation of earlier single-image speckle-interferometric observations by Keller (1992), established conclusively that magnetic flux is a necessary but not sufficient condition for the occurrence of photospheric bright points and filigree. In other words, while bright points occur without exception at sites of magnetic flux (to the limiting spatial resolution of the magnetograms of about 0".5), there are sites of magnetic flux which do not appear to have any associated bright points. The main problem with the observations of both Yi & Engvold (1993) and Keller (1992) is that small-scale flux elements exhibit very low contrast in continuum wavelengths near disk center; only the brightest elements in larger intergranular dark spaces are clearly observable in their data. This limits the applicability of their methods to a subset of the full size and brightness range of magnetic elements found in the photosphere.

In 1993 August a 12 Å bandpass interference filter, centered at 4305 Å in the Fraunhofer "G band," was added to a secondary beam line of the SVST in an attempt to extend the bright point observations of Yi & Engvold (1993). The G band filter was designed to replicate the results of Muller & Roudier (1984), who had shown that images in this particular molecular bandhead exhibit bright points with higher contrast than that found in continuum wavelengths. Although the SVST filter has a bandpass only slightly different from that used by Muller & Roudier (1984), bright points in the images exhibit contrast values 2–3 times those measured in the earlier studies. As a result, numerous bright points on a wide range of brightness and size scales are

[1] There is evidence for an additional weak field component which is seen, for example, at the center of supergranular cells (Livingston & Harvey 1975; Martin 1984; Martin 1988; Martin 1990; Wang, Zirin, & Shi 1985; Zirin 1987). Estimates of the strength of this field component vary from less than 100 G (Tarbell, Title, & Schoolman 1979) to less than 500 G (Keller et al. 1994) on spatial scales of 2"–5".

easily identifiable among complex granular fields at disk center for the first time. Berger et al. (1995) used images taken with this filter to compile statistical data on the properties of small-scale magnetic elements on 0".25 spatial scales. In addition, concurrent G band and SOUP magnetogram time series analyses (Berger et al. 1996) have verified the conclusions of Yi & Engvold (1993), and also established that photospheric bright points occur preferentially on the periphery of strong field concentrations, in regions in which the field is distended in narrow "arms" from stronger concentrations, and in isolated sub-0".5 structures (Berger et al. 1996). The conclusion is that G band images are a reliable "proxy" for some fraction of the small-scale magnetic flux in the photosphere. Exactly what fraction of the small-scale field, and exactly which magnetic sites, will be represented with G band bright points at any given time is uncertain; the mechanism of G band brightening in small-scale magnetic elements, and why some elements are illuminated while others are not, is not understood. However, since G band image time series have much higher spatial and temporal resolution than any magnetograms currently produced by ground-based instruments, it has become clear that studies of small-scale magnetic field dynamics can be best accomplished using G band images.

This paper presents the first results from analyses of a long time series of bright-point images taken with the new G band filter. In the following sections we describe the observational, image processing, and analysis techniques which have been applied to the time series to produce new impressions of the dynamic nature of small-scale magnetic flux in the solar photosphere.

2. OBSERVATIONS

All observations presented here were acquired in the summer of 1994 at the SVST (Scharmer et al. 1985), a 50 cm f/45 doublet vacuum refractor located 2400 m above sea level on the island of La Palma, Spain. The prime-focus instrumentation consists of a 3 Å wide Ca II K line interference filter directly in front of a Kodak Megaplus 1.4 CCD camera (1360 × 1036 6.4 μm pixel format, lumigen coated, run at room temperature). The prime-focus plate scale for all observations discussed here is 15.92 pixels arcsec^{-1}, with a nominal field of view of 80" × 65". A second beam is split off the prime-focus beam and reimages the Sun with 1:1 magnification through the 12 Å bandpass G band interference filter onto an additional (noncoated) Megaplus 1.4. A third beam reimages the Sun at 1:1 magnification through the SOUP filter and onto a Kodak Megaplus 1.6 CCD camera (1534 × 1024 9 μm pixel format). The plate scale on the Megaplus 1.6 camera is approximately 12 pixels arcsec^{-1}.

The Megaplus 1.4 cameras are controlled and read by a single Digital Equipment Corporation (DEC) Alpha workstation using a custom high-speed digital interface board (Shand 1995). Another Alpha workstation and digital interface board link is used to control the Megaplus 1.6 camera and trigger the SOUP filter sequences. Minimum exposure time on all cameras is 10 ms. Typical frame readout time for the Megaplus 1.4 cameras is 130 ms, resulting in a maximum sustained frame rate of approximately 7 frames s^{-1}. On all cameras, a 256 × 256 pixel^2 subarea of the image is evaluated in real time for contrast sharpness; the image with the highest sharpness index value during a user-selected "evaluation period" is written to 8 mm tape. Since the acquisition time of the best image is random within the evaluation period, the images are not regularly spaced in time; for a 10 s evaluation period the maximum time between frames is about 20 s.

The choice of evaluation period depends on the seeing, as well as on the goal of the observing program. In poor seeing, a longer period is used in order to "wait" for the best image and avoid writing blurred images to tape. Conversely, in good seeing a shorter period is used in order to maximize temporal resolution of the image series. In the best seeing conditions, evaluation periods of between 10 and 20 s are used. Variable seeing conditions usually require a 20–30 s period in order to produce useful image series. The evaluation period is defined as the nominal "temporal resolution" of the filtergram image series because it approximates the mean time between images in the set. However, images spaced significantly less in time than this value are common in any set. The temporal resolution of the SOUP image series is defined differently than, and is somewhat lower than, the corresponding filtergram temporal resolution. Specifically, the SOUP filter is run in a cycle which may observe in several wavelength regimes in order to obtain, for instance, magnetograms, Dopplergrams, and continuum images in sequence. Each wavelength regime goes through a frame selection period, and additional time is required to rotate the blocking filters, polarization filters, and wave-plate elements within the SOUP filter itself in order to change wavelength. As a result, the mean time between images in a single SOUP wavelength regime is typically a factor of 2 or 3 longer than in the G band image series.

The primary time series analyzed here is a 10 hr observation of NOAA Active Region 7731 observed near disk center (9N 3W; $\mu = 0.99$) on 1994 June 14. The active region is a decaying single-spot complex with a pronounced moat region, one area of which contains a large pore complex. The pore complex shares the same polarity as the main spot, while the remainder of the moat is composed of opposite polarity plage. Images were acquired in two series from 07:00 UT to 11:20 UT and from 11:30 UT to 17:40 UT, with a 20 s evaluation period for the Ca II K line and G band cameras. The SOUP filter sequence was MESO1, which cycles through a Fe I 5250 Å magnetogram image pair, a Fe I 6302 Å magnetogram pair, a Fe I 5576 Å Doppler image pair, and a 6328 Å continuum image. Figure 1 (Plate 25) shows a G band image of the region taken at 08:24 UT with an exposure time of 23 ms. The image is nearly diffraction-limited across the entire field of view. The modal FWHM diameter of the bright points in the image is 0".25. A detailed study of the static properties of these bright points, including their relation to the magnetic field, is contained in Berger et al. (1996).

3. IMAGE PROCESSING

Standard CCD-camera image postprocessing is performed on each raw image written to tape by the frame-selection system: dark noise subtraction and flat fielding are followed by image alignment and derotation in order to correct for the image motion imposed by the altitude-elevation mount of the SVST. Two-dimensional bilinear interpolation is also applied to any flawed pixels in the image. Each monochromatic image set is then rigidly aligned using local two-dimensional cross correlation to compensate pointing and/or tracking drift errors. Follow-

ing rigid alignment, each image set is "destretched" (Topka, Tarbell, & Title 1986; November 1986) to a running average reference image in order to remove geometric distortions due to seeing. This procedure, like all interpolative operations on images, has the effect of reducing spatial resolution but, for image sets taken in good seeing, the reduction is estimated to be less than 0".05.

Zeeman effect magnetograms are created by subtracting images taken by the SOUP filter in left circularly polarized (LCP) and right circularly polarized (RCP) light from the wings of either the Fe I 5250 Å or 6302 Å absorption lines (Title, Tarbell, & Topka 1987). Typical exposure times for the narrow-bandwidth (82 mÅ in the Fe I 5250 Å line) SOUP magnetogram images are 50–100 ms. The resulting image shows the degree of circular polarization at a given location in the photosphere (averaged over the resolution element defining the minimum spatial resolution) which is proportional to the longitudinal magnetic flux density at the location. Since we are primarily interested in the dynamics of the magnetic field in this study and not its absolute magnitude, field strength values (which are difficult to determine accurately anyway due to imprecisely known calibration constants; Title et al. 1987) were not calculated from the polarization images. The LCP and RCP images are not exactly simultaneous and are affected by differing degrees of atmospheric distortion and blurring. Therefore, the SOUP magnetogram spatial resolution is never as good as the spatial resolution obtained in the single-image filtergrams. Nevertheless, it is clear from detailed examination of the magnetograms obtained in AR 7731 1994 June 14 that we are resolving individual magnetic elements 0".4–0".5 in diameter and perhaps smaller. Therefore, we feel confident that we can correlate G band bright-point dynamics, at least on a 0".4 spatial scale, with changes in the magnetogram images. The SOUP filter cycle used a 10 s evaluation period; the resulting mean time between images for the 1994 June 14 magnetograms is 42 s, with a maximum of 48 s and a minimum of 37 s.

Following processing of each monochromatic time series, the sets are coaligned and scaled to a common plate scale using on the order of 10–20 points which are clearly identified as common features in all image sets. All image sets presented here were aligned and scaled to the G band image set and therefore have a nominal plate scale of 15.92 pixels arcsec^{-1}. A least-squares calculation solves the overdetermined matrix equation for the affine transformation used for the final processing of each image in the time series. Since the magnetogram images do not contain structures which are sufficiently similar to structures in the other image sets, the transformation applied to the 6328 Å SOUP filter continuum images was automatically applied to the magnetograms. The geometric alignment and scaling result in residual alignment errors between image sets of up to 0".1.

4. RESULTS

The main result gained from study of the G band time series is that the concept of the small-scale solar magnetic field being contained in stable flux tubes of relatively constant shape is completely invalid in active region plage and is probably equally inapplicable to the network regions as well. A localized magnetic element cannot be defined as a unique structure for longer than a typical granule lifetime (6–8 minutes). This is because the shape of individual bright points, their number density, and their interaction with other bright points are strongly dependent on the local granular convective flow field. Four main evolutionary effects are seen as a result of the interaction of magnetic elements with the granular flow field:

1. Elongation or other significant shape modifications including rotation and folding.
2. Motion along the (evolving) intergranular lane environment. Typical speeds are from 1 to 5 km s^{-1}, and distances of travel vary from 1 to several granular diameters.
3. Merging of one or more elements to form a larger element, usually at a convergence point in the granular flow field.
4. Splitting of a larger element into 2, or in most cases, several smaller elements.

It is typical for any individual element which may be chosen in a single frame of the time series to undergo all of these modes of behavior during the time it, and its associated "relatives," can be recognized. Earlier observations by Sheeley (Sheeley 1969; Sheeley 1971) in the 3883 Å bandhead of the CN molecule had indicated such dynamic behavior of bright points on 1" spatial scales. Similar fragmentation/merging evolution has also been detected in the chromospheric network structures seen in the Ca II K line at much larger spatial scales (Schrijver et al. 1995).

A good analogy for the appearance and behavior of small-scale magnetic flux in the photosphere is that of drops of a high surface tension immiscible oil floating on the surface of a convective fluid. As the surface convection pattern evolves, an individual oil droplet moves along the troughs in the fluid until it meets another oil drop. At this point, the drops either merge, bounce off one another, or merge and then immediately fragment into two or more droplets. The trough pattern, which is itself continually evolving, is a complex network of branches connected at vertices. When a drop reaches a vertex in the network, it may fragment and the droplets may travel into different branches from the vertex. It may also settle into the vertex and maintain a relatively stable position for some time while undergoing continual shape changes and rotations. When a new convective cell moves into a trough containing a drop, the trough will be compressed and the drop will elongate along the thinned trough. If the strain induced in the drop—due to the elongation—exceeds the surface tension, the drop will break into several droplets which may travel in different directions along the evolving trough. If one were to tag a given drop with a dye, it is likely that, in time, an increasing number of dyed droplets would be found in the flow field as the fragments of the original drop disperse in the flow field. The range of travel of the fragments over time would most likely be on the order of several convective cell diameters, but could possibly span many more.

In the case of solar magnetic elements, the droplets represent the flux concentrations, the troughs in the convective flow field are the intergranular lanes, and the vertices are sinks in the flow field. We observe that it is rare for elements to merge to form a structure with a diameter that is large compared to the width of the intergranular lanes. Merging of magnetic elements takes place in complex ways that include the folding of an elongated chain of elements onto itself, thereby creating a large structure. This is seen when a granule collapses and two branches surrounding the cell

fold inward and merge. There are also cases in which elements approaching a vertex from different directions possess relative angular momentum which is manifested in a vortex-like motion of the larger element formed in the merging of the smaller ones. We also observe that elements at the limit of the spatial resolution of the images sometimes appear to disappear in an intergranular lane. This can be explained by hypothesizing that the element has further fragmented into subresolution structures which are too small to observe. Berger et al. (1995) showed that the number distribution of G band bright points in plage increases with decreasing size, with an indication of a peak at or near the diffraction limit of the 50 cm SVST. The implications of this finding and of the movie observations are that the magnetic elements which are seen to fade from view do not cease to exist but are simply too small to be resolved by a 50 cm telescope. Title & Berger (1996) have shown that small bright objects in dark surroundings (such as the intergranular lanes) have an integrated contrast which is usually less than the mean surface intensity; when a magnetic element becomes too small, it is effectively "averaged" into the intergranular lane by the telescope point-spread function, and thus becomes indistinguishable from the dark surrounding. Conversely, we occasionally see an apparently spontaneous creation of a flux element in a vertex of the granular flow field, which may indicate merging of subresolution elements to form the observed structure.

Because of the dynamic nature of the convective flow field, the "lifetime" of any given magnetic element is very difficult to define. If one starts by selecting a "large" bright point in a convergent point in the granular flow field in one image, for example, it is likely that the point will be fragmented into at least two smaller points within a period on the order of 5 minutes. Typically, these smaller points will move within the constantly changing intergranular lanes until another convergence point (perhaps at or very near to the original one) evolves in the local flow field. The smaller points may then merge to re-form the larger structure. In this example, the total magnetic flux observed in the initial image is conserved, but is temporarily redistributed into structures which, in any single image taken at the proper moment, would be identified as completely different elements of the field. Also, previously reported values for average bright-point lifetimes on the order of 18 minutes (Muller 1983) may be understood as owing to a large time gap between images in a sequence: bright points observed at slow cadence, especially in sinks in the flow field, will appear to be more stable than they actually are. If it is possible to define the dynamic lifetime of small-scale magnetic elements at all, it is probably best defined in terms of the stability and lifetime of the intergranular sinks, which collect and trap the most persistent flux elements in the time series. In the 1994 June 14 time series, convergent points in the flow field (as identified by the presence of magnetic elements which undergo continual fragmentation and merging in a relatively stable location) are observed to persist for periods of several hours. The complexity of motions seen in our observations call into question any definition of lifetime one may give for any amount of flux in the small-scale field.

The above descriptions of dynamic events are difficult to illustrate with still images. However, with the descriptions in mind, it is possible to examine selected image sequences from the movies and see the evolutionary behavior occurring in steps. Figures 2, 3, and 4 (Plates 26–28) show such sequences in G band, Ca II K line, and magnetogram images, respectively; the temporal registration between the sets is very good in the case of the G band and the Ca II K line. In the case of the magnetogram movie, the longer cadence imposed by the SOUP filter results in fewer images of the required quality to choose from in the time period corresponding to the G band and K line movies. The sequence shown was chosen to illustrate the evolution of a large $\sim$0.″35 bright point that appears near the center of the earlier images in the sequence. Although the bright point appears to rotate in place (changing by perhaps 90° between 13:27:01 and 13:32:03), the actual dynamic behavior seen in the movie is more complex: the granule to the right of the bright point expands into and creates a crease in the flux element, and the two "arms" of the element then elongate toward the vertical. Another such granule collision is seen in the 13:20:24 frame, in which the granule expands from the upper left. The following frame taken at 13:22:12 shows that the bright point has been fragmented by the collision into at least three smaller elements. They appear to merge to form a single element again by 13:25:07. The magnetogram sequence for the same time interval confirms the existence of a highly concentrated flux element at the location of the bright point. However the lower spatial resolution does not reveal any substructure, although changes in the shape of the flux concentration are evident.

After 13:30:23, the bright point evolves more radically. By 13:38:28 the bright point has elongated into a chain of several small elements that is approximately 2″ long. The smallest elements are no more than 0.″25 in diameter. At 13:40:41 the chain has increased in brightness and there is an indication that fragments have broken off and moved toward the lower right-hand area of the image. By 13:45:07 the chain has split into two groups, which continue to separate and evolve individually. The elements on the left-hand side move toward the lower left, and by 13:47:17 they have encountered another flux group. At 13:51:16 these elements have become two well-localized bright points which are easily seen in the Ca II K line image sequence as well. Finally, at 13:55:01, the final frame of the sequence, the two points in this group merge to form the large bright point at the left-center area of the image. The other group from the original splitting has formed a complex chain structure in the upper right-hand side of the image. In the time span of less than 15 minutes, a compact magnetic element has evolved into two well-separated groups, both of which contain flux from other preexisting elements. The image sequences shown in Figures 2–4 illustrate typical behavior of the small-scale magnetic flux throughout the mature active region shown in Figure 1.

5. CONCLUSIONS

We have established that the small-scale magnetic flux in active region plage is in a highly dynamic state. The main conclusion is that the concept of an isolated, relatively stable, or even oscillating flux tube, with a lifetime longer than granulation, is not consistent with the observations. Flux that is located within a particular element at a given time will most likely be redistributed to other elements on a timescale of 6–8 minutes. On timescales on the order of 100 s or less, significant morphological changes occur to all

small-scale magnetic elements in an active region. Although we lack data from the quiet network, the similarity of the granular convective flow field and the existence of small-scale magnetic elements in this flow field lead us to believe that the evolution of network bright points will be very similar to that observed in the plage regions.

The dominant modes of small-scale magnetic flux evolution in the photosphere are fragmentation and merging. This result has ramifications for theories of flux topology both above and below the photosphere. Above the photosphere, the speed and range of motion of magnetic flux elements are crucial parameters in theories of episodic atmospheric heating based on the reconnection of twisted magnetic field lines (van Ballegooijen 1986; Parker 1988; Parker 1990; Sturrock et al. 1990; Muller et al. 1994). We observe motion of small-scale magnetic elements in the photosphere on spatial scales of arcseconds (1000 km) with velocities from 1 to 5 km s^{-1}. This is in line with the results of Muller et al. (1994), who have measured an average bright-point speed of 1.4 km s^{-1} and a maximum speed of 3 km s^{-1} in quiet network regions. Previous models (Parker 1990) have assumed speeds of 0.5 km s^{-1} (based on the observed speed of granular advection in the photosphere) over characteristic distances of several hundred kilometers. However, the speeds and range of motion reported here imply that in Parker's model, for a given tangential discontinuity threshold at which the field reconnects and releases energy, the power input into the corona is an order of magnitude higher than previously calculated. Conversely, if the power input is kept constant at the value necessary to heat the X-ray corona (Withbroe & Noyes 1977), our observations imply that the angular discontinuity threshold in the field at which reconnection occurs is even lower than the range of 10°–15° calculated by Parker (1990). The motions of magnetic "footpoints" that we measure are more energetic and complex than previously observed, with the consequence that the hypothesis of coronal heating by the episodic nanoflare mechanism is made more plausible.

An additional consequence of the dynamic behavior we observe in photospheric bright points is the creation of large currents caused by the time dependence of the magnetic field. As a simple estimate of the current density caused by the splitting of a small-scale magnetic element, we model the element as an ideal linear solenoid, vertically oriented in the photosphere. We assume the diameter of the solenoid is 250 km and that it undergoes a binary splitting into two identical (equal area, equal field strength) fragments. Consider a circuit closely enclosing the original element. Assuming that the initial field strength is 1500 G and is uniform across the area of the element, let one fragment move a distance greater than 250 km from the original location (i.e., out of the circuit) in about 100 s (an implied speed of 2.5 km s^{-1}). Assuming the conductivity is 100 A m^{-1} in the lower photosphere (Kopecký & Soytürk 1971), an azimuthal current density on the order of 10^4 A m^{-2} is induced in the circuit. Because of the complex nature of the conductivity in the convective plasma of the photosphere, actual current densities induced by such splitting are expected to be lower than that calculated above. More detailed calculations (based, however, on values of the flow velocity in the neighborhood of flux elements that are somewhat lower than we observe) would appear to verify this expectation: Hirayama (1992) calculates an azimuthal current density in a thin flux tube model (with a uniform horizontal velocity inflow and similar geometric and magnetic field assumptions to those made above) on the order of 100 A m^{-2}; work in progress using plasma-dynamic models of the interaction of the magnetic element internal gas with the granular acoustic field also produces azimuthal current densities on the order of 10–100 A m^{-2}. We conclude that actual azimuthal current densities in small-scale magnetic elements in the photosphere are between 10^2 and 10^4 A m^{-2}. The effects of current densities of this order of magnitude on the interior atmospheres of magnetic elements are not known. Previous studies have indicated that current systems within flux tubes may have very significant effects on the gasdynamics within and immediately outside flux tubes (Hirayama 1992; Henoux & Somov 1994).

Below the photosphere, fragmentation and merging dynamics have implications for theories of flux emergence and pore and sunspot formation. It is still uncertain whether concentrated flux tubes such as pores emerge as coherent elements from the convection zone, or whether they are formed from coalescence of preexisting small-scale magnetic elements in the photosphere. The observations analyzed here tend to refute the latter hypothesis; in none of our movies do we observe merging of small-scale bright points to form pores, nor do we observe small pores fragmenting into bright points. In fact, the pores which exist in our data are stable throughout the time series and undergo only slight changes around their peripheries due to interactions with the granular flow field. It is possible that pore formation occurs from the coalescence of larger dark magnetic elements (e.g., micropores; see Topka, Tarbell, & Title 1992), which in turn may be formed from merging bright points. However, we cannot detect micropore formation in our data reliably, and so we cannot support or refute this hypothesis. What is clear is that there is often enhanced number density of bright points around small pores; in several instances we observe small pores completely ringed by a static configuration of sub-0".5 bright points. The configuration of these bright points and their often radially elongated shape is reminiscent of penumbrae around sunspots and may be evidence of "protopenumbrae" formation. But the nature of the dynamic interaction of magnetic elements across a wide size range (from bright points to sunspots) remains unclear.

Producing more quantitative results than those shown here is desirable. However, production of statistical results from bright-point proxy observations requires seeing of 0".3 or better over long periods of time; such observations are not yet possible using ground-based instrumentation. Investigations into phase-diversity image reconstruction (Löfdahl & Scharmer 1994; Paxman, Schulz, & Fienup 1992) are underway in order to improve the uniformity of spatial resolution across long time series. Direct observation and measurement of small-scale solar magnetic field dynamics (i.e., as distinct from proxy observations) can only be done with magnetograms from a 1 m class space-based telescope.

This work was supported by NASA contracts NAS 5-30386 at Stanford and NAS 8-39747 and Independent Research Funds at Lockheed-Martin. The SVST is operated by the Swedish Royal Academy of Sciences at the Spanish Observatorio del Roque de los Muchachos of the Instituto de Astrofisica de Canarias (IAC). We thank

George Simon and Peter Brandt for their outstanding observing skills exhibited in obtaining the 1994 June 14 time series. Dick Shine and Zoe Frank performed the initial data reduction and image set alignment. Karel Schrijver, Ted Tarbell, and Dick Shine provided many helpful comments and suggestions. Goran Scharmer, Paco Armes, Göran Hosinsky, Rolf Kevar, and Wong Wei of the Swedish Solar Observatory maintain the SVST in its status as one of the premiere solar telescopes in the world. Mary Baretto and the staff of the IAC are thanked for providing excellent accommodations and assistance on this and all previous observing campaigns at La Palma.

REFERENCES

Beckers, J. M., & Schröter, E. H. 1968, Sol. Phys., 4, 142
Berger, T. E., Schrijver, C. J., Shine, R. S., Tarbell, T. D., Title, A. M., & Scharmer, G. 1995, ApJ, 454, 531
———. 1996, in preparation
Chapman, G., & Sheeley, N. R. 1968, Sol. Phys., 5, 442
de Boer, C. R., & Kneer, F. 1992, A&A, 273, 304
Dunn, R. B., & Zirker, J. B. 1973, Sol. Phys., 33, 281
Frazier, E. N., & Stenflo, J. O. 1972, Sol. Phys., 27, 330
Harvey, J. W., & Hall, D. N. B. 1975, BAAS, 7, 459
Henoux, J. C., & Somov, B. V. 1994, in Solar Active Region Evolution: Comparing Models with Observations, Vol. 68, ed. K. S. Balasubramaniam & G. W. Simon (San Francisco: ASP), 158
Hirayama, T. 1992, Sol. Phys., 137, 33
Howard, R., & Stenflo, J. O. 1972, Sol. Phys., 22, 402
Keller, C. 1992, Nature, 359, 307
Keller, C. U., Deubner, F.-L., Egger, U., Fleck, B., & Povel, M. P. 1994, A&A, 286, 626
Keller, C. U., Solanki, S. K., Tarbell, T. D., Title, A. M., & Stenflo, J. O. 1990, A&A, 236, 250
Kopecký, M., & Soytürk, E. 1971, Bull. Astron. Inst. Czechoslovakia, 22, 154
Livingston, W., & Harvey, J. W. 1975, BAAS, 7, 346
Löfdahl, M. G., & Scharmer, G. B. 1994, A&AS, 107, 243
Martin, S. F. 1984, in Small-Scale Dynamical Processes in Quiet Stellar Atmospheres, ed. S. L. Keil (Sunspot: NSO), 30
———. 1988, Sol. Phys., 117, 243
———. 1990, in IAU Symp. 138, Solar Photosphere: Structure, Convection and Magnetic Fields, ed. J. O. Stenflo (Dordrecht: Kluwer), 129
Mehltretter, J. P. 1974, Sol. Phys., 38, 43
Muller, R. 1975, Sol. Phys., 45, 105
———. 1983, Sol. Phys., 85, 113
———. 1994, in NATO ASI, 433, Solar Surface Magnetism, ed. R. J. Rutten & C. J. Schrijver (Dordrecht: Kluwer), 73
Muller, R., & Keil, S. L. 1983, Sol. Phys., 87, 243
Muller, R., & Roudier, T. 1984, Sol. Phys., 94, 33
Muller, R., Roudier, Th., Vigneau, J., & Auffret, H. 1994, A&A, 283, 232
November, L. J. 1986, Appl. Opt., 25, 392
Parker, E. N. 1988, ApJ, 330, 474
———. 1990, in Mechanisms of Chromospheric and Coronal Heating, ed. P. Ulmschneider & E. R. Priest (Berlin: Springer), 615
Paxman, R. G., Schulz, T. J., & Fienup, J. R. 1992, J. Opt. Soc. Am., A, 9, 1072
Rabin, D. 1992, ApJ, 390, L103
Ryutova, M. P., Kaisig, M., & Tajima, T. 1996, ApJ, 459, 744
Scharmer, G. 1989, in NATO ASI 263, Solar and Stellar Granulation, ed. R. J. Rutten & G. Severino (Dordrecht: Kluwer), 161
Scharmer, G. B., Brown, D. S., Petterson, L., & Rehn, J. 1985, Appl. Opt., 24, 2558
Schrijver, C. J., et al. 1995, ApJ, submitted
Shand, M. 1995, in Proc. IEEE Workshop on FPGAs for Custom Computing Machines, 17
Sheeley, N. R. 1971, Sol. Phys., 20, 19
———. 1967, Sol. Phys., 1, 171
———. 1969, Sol. Phys., 9, 347
Simon, G. W. 1994, in NATO ASI 433, Solar Surface Magnetism, ed. R. J. Rutten & C. J. Schrijver (Dordrecht: Kluwer), 261
Simon, G. W., & Zirker, J. B. 1974, Sol. Phys., 35, 331
Solanki, S. K. 1993, Space Sci. Rev., 63, 1
Spruit, H. C. 1976, Sol. Phys., 50, 269
Spruit, H. C., & Zweibel, E. G. 1979, Sol. Phys., 62, 15
Steiner, O., Grossman-Doerth, V., Knölker, M., & Schüssler, M. 1994, in Rev. Mod. Astron., ed. G. Klare (Hamburg: Astronomische Gesellschaft), 17
Stenflo, J. O. 1973, Sol. Phys., 32, 41
Stenflo, J. O., & Harvey, J. W. 1985, Sol. Phys., 95, 99
Sturrock, P. A., Dixon, W. W., Klimchuk, J. A., & Antiochos, S. K. 1990, ApJ, 356, L31
Tarbell, T. D., & Title, A. M. 1977, Sol. Phys., 52, 13
Tarbell, T. D., Title, A. M., & Schoolman, S. A. 1979, ApJ, 229, 387
Title, A. M., & Berger, T. E. 1996, ApJ, in press
Title, A. M., & Rosenberg, W. J. 1981, Opt. Eng., 20, 815
Title, A. M., & Tarbell, T. D. 1975, Sol. Phys., 41, 255
Title, A. M., Tarbell, T. D., & Topka, K. P. 1987, ApJ, 317, 892
Title, A. M., Tarbell, T. D., Topka, K. P., Ferguson, S. H., Shine, R. A., & The Soup Team. 1989, ApJ, 336, 475
Title, A. M., Topka, K. P., Tarbell, T. D., Schmidt, W., Balke, C., & Scharmer, G. 1992, ApJ, 393, 782
Topka, K. P., Tarbell, T. D., & Title, A. M. 1986, ApJ, 306, 304
———. 1992, ApJ, 396, 351
van Ballegooijen, A. 1986, ApJ, 311, 1001
Wang, J., Zirin, H., & Shi, Z. 1985, Sol. Phys., 98, 241
Withbroe, G. L., & Noyes, R. W. 1977, A&A Rev., 15, 363
Yi, Z., & Engvold, O. 1993, Sol. Phys., 144, 1
Zayer, I., Solanki, S. K., & Stenflo, J. O. 1989, A&A, 211, 463
Zirin, H. 1987, Sol. Phys., 110, 101

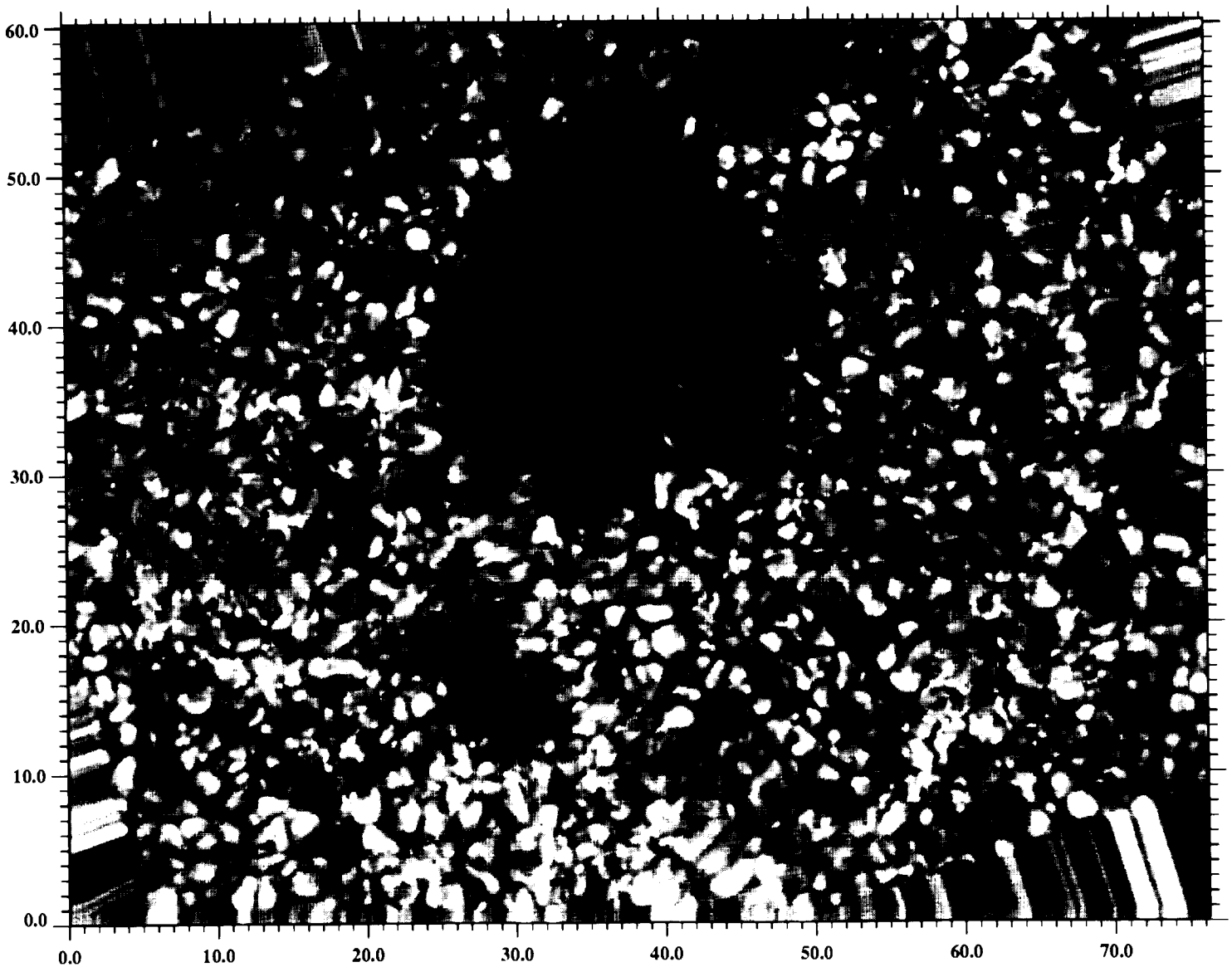

FIG. 1.—NOAA Solar Active Region 7731 imaged on 1994 June, 14 at 08:24 UT near disk center with the Swedish Vacuum Solar Telescope on La Palma, Spain. The filter is a 12 Å bandpass interference filter centered at 4305 Å in the G band. The detector is a Kodak Megaplus 1.4 camera, exposure 15 ms, plate scale 16 pixels arcsec^{-1}. Tick marks are arcseconds. The linear artifacts at the edges are due to image rotation imposed in the postprocessing.

BERGER & TITLE (see 463, 367)

PLATE 25

PLATE 26

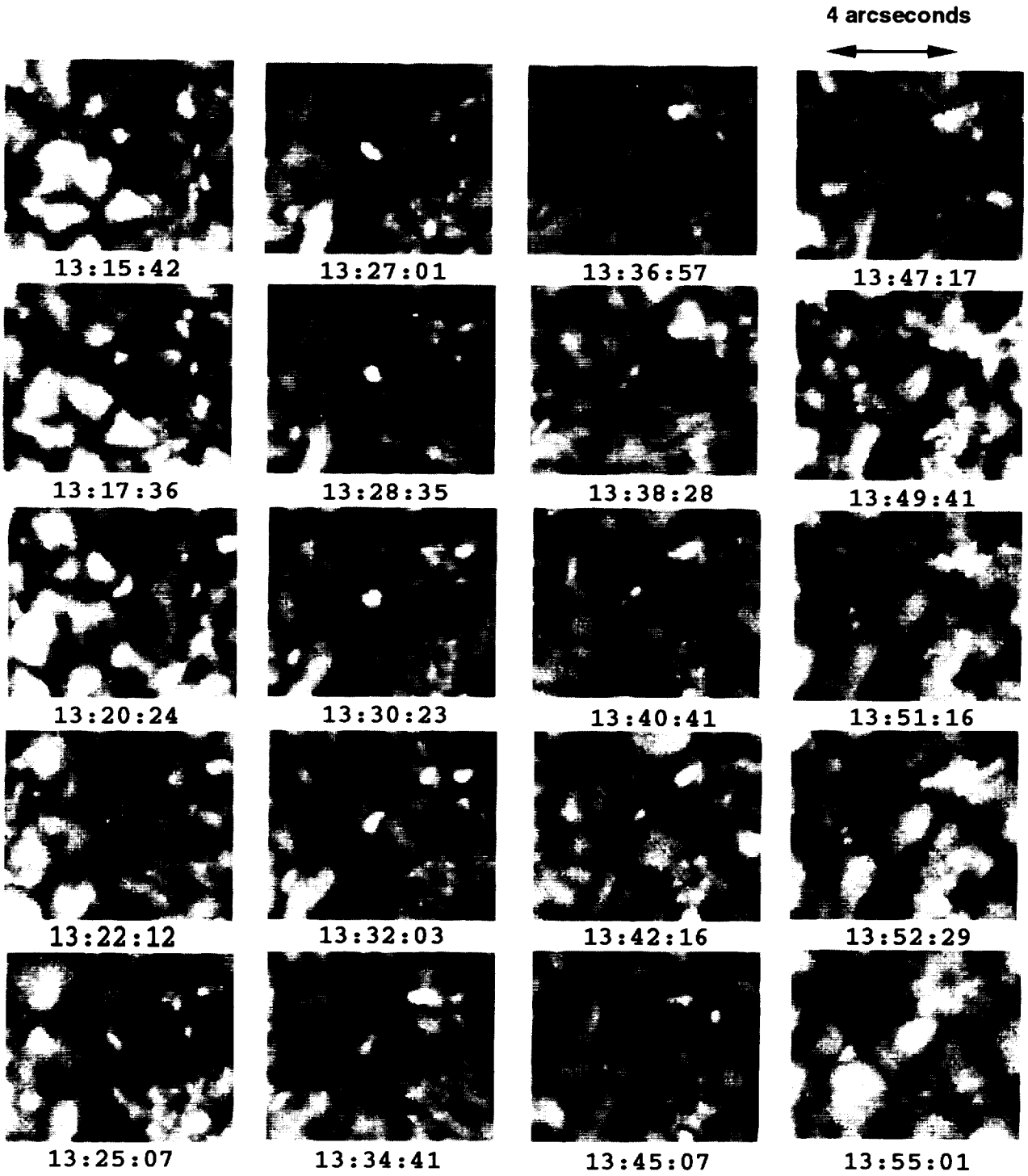

FIG. 2.—Time series of G band images taken from an area of the active region shown in Fig. 1. Times are UT, increasing in columns from upper left. Image scale is indicated by the 4"-long arrow. Note the changes to the central bright point due to the interaction with the granular convective flow field.

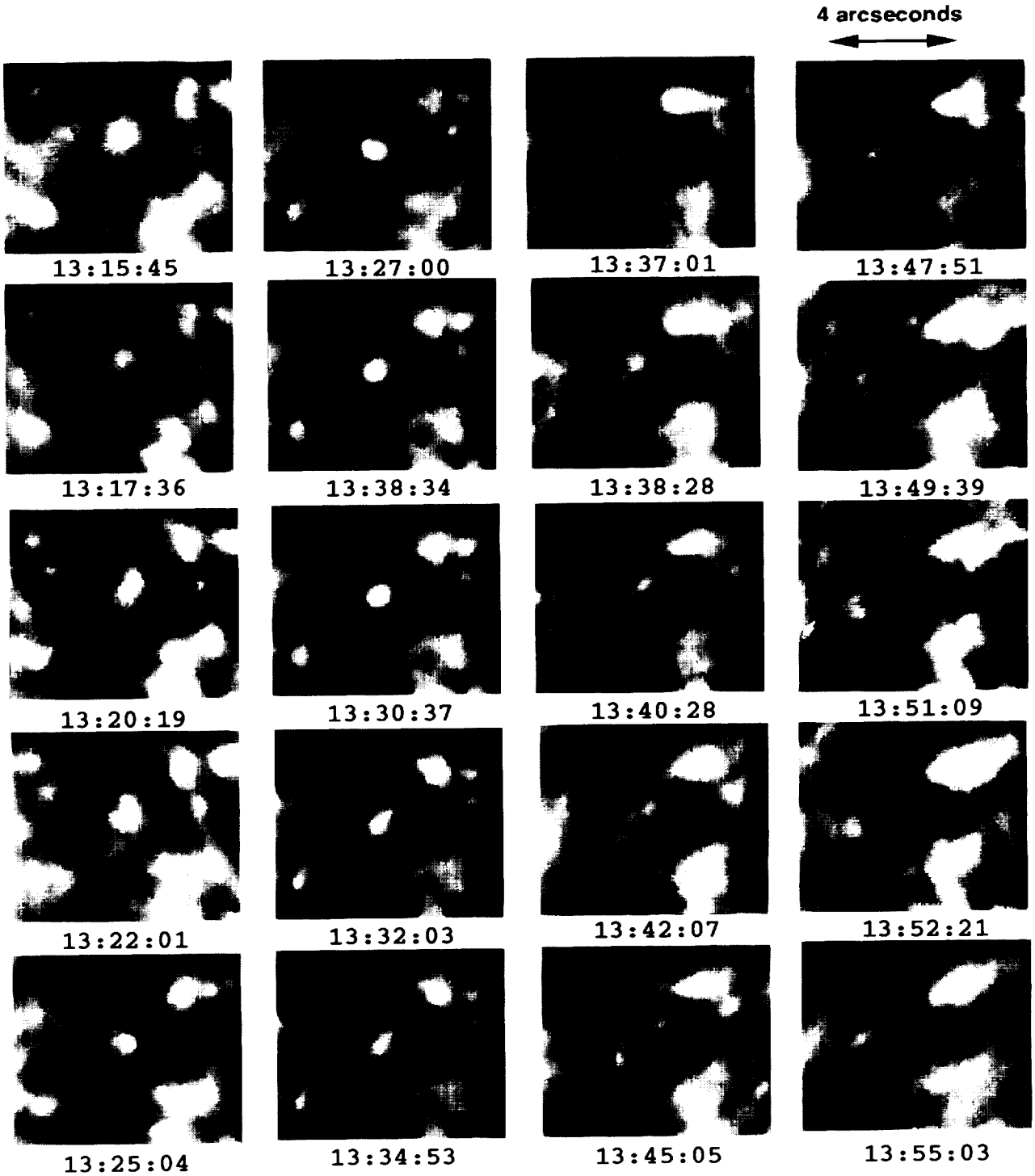

FIG. 3.—Time series of Ca II K line images of the same area shown in Fig. 2. Times are UT, increasing in columns from upper left, and correspond closely to times in Fig. 2. The morphological changes seen in the G band image series are detectable in this series as well, but with slightly lower spatial definition: the splitting and merging seen in the photospheric G band images also occur at the level of Ca II K line formation, which is somewhat higher in the solar atmosphere.

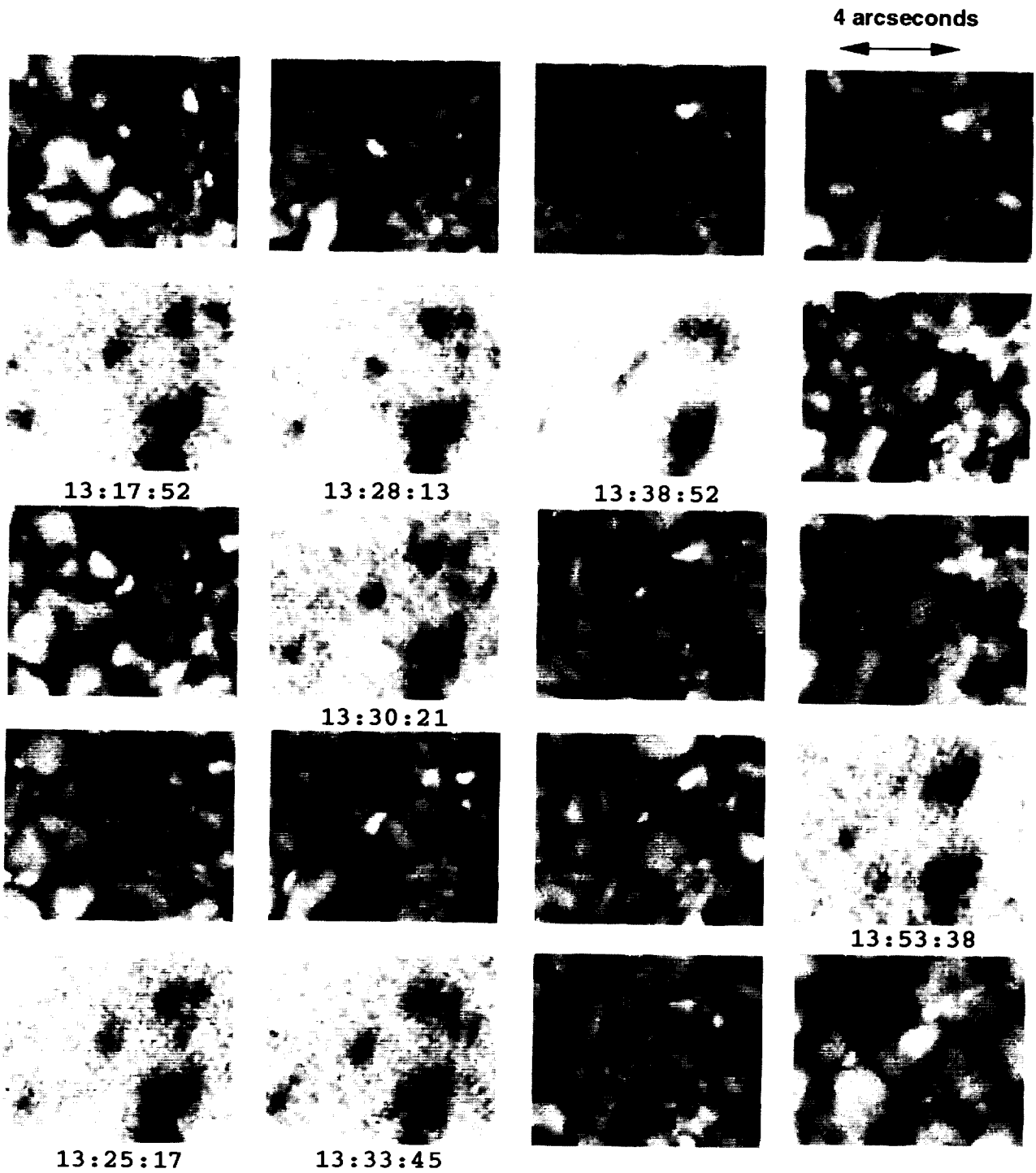

FIG. 4.—Time series of Fe I 6302 Å magnetogram images of the same area shown in Fig. 2. Times are UT, increasing in columns from upper left. Gaps in the time series have been filled with G band images from Fig. 2. Although lower in spatial resolution, the magnetogram images confirm that elongation and splitting of G band bright points occur simultaneously with the same morphological changes in the magnetic field.